Quaternary Science Reviews 295 (2022) 107783

Contents lists available at ScienceDirect

Quaternary Science Reviews

journal homepage: www.elsevier.com/locate/quascirev

Probabilistic investigation of global mean sea level during MIS 5a based on observations from Cave Hill, Barbados

Kai Tawil-Morsink [a, b, c, *], Jacqueline Austermann [b, c], Blake Dyer [d], Oana A. Dumitru [b], William F. Precht [e], Miranda Cashman [b, c, f], Steven L. Goldstein [b, c], Maureen E. Raymo [b, c]

[a] Department of Earth and Planetary Sciences, Harvard University, Cambridge, MA, 02138, USA
[b] Lamont-Doherty Earth Observatory, Columbia University, Palisades, NY, 10964-8000, USA
[c] Department of Earth and Environmental Sciences, Columbia University, Palisades, NY, 10964, USA
[d] School of Earth and Ocean Sciences, University of Victoria, Victoria, BC V8W 2Y2, Canada
[e] Dial Cordy and Associates Inc., Coastal and Marine Programs, Miami, FL, 33179, USA
[f] New York City Department of Environmental Protection, Flushing, NY, 11373, USA

ARTICLE INFO

Article history:
Received 21 January 2022
Received in revised form
20 May 2022
Accepted 19 September 2022
Available online 2 October 2022

Handling Editor: Dr I Hendy

ABSTRACT

Global mean sea level (GMSL) reconstructions from past interglacial periods help us understand the sensitivity of ice sheets to a warming climate. In this study, we focus on Marine Isotope Stage 5a (MIS 5a), a warm period that peaked 82,000 years ago and for which current GMSL estimates remain widely uncertain (ranging from −28 m to +1 m). Here we reconstruct relative sea level (RSL) based on an extensive and exquisitely preserved fossil coral reef at Cave Hill, Barbados, which has not been examined before. We dated one coral sample (*Acropora palmata*) from this outcrop using U-series dating and obtained a closed system age of 82.5 ± 0.4 ka and an open system age of 83.3 ± 0.7 ka (2σ), which confirm that the reef formed during MIS 5a. We determine RSL based on the elevation of 222 fossil corals within the outcrop from three species (*Acropora palmata*, *Siderastrea radians*, *Favia fragum*). The coral elevations are combined using Bayesian inference to obtain a posterior common RSL, with present-day water depths of each species as priors. We use our inference scheme and synthetic datasets to explore the number and species of corals needed for a robust RSL estimate and find that if approximately 5 corals are sampled, roughly half of which have a narrow living depth range (0 to ~10 m), the accuracy and precision of the inferred RSL is around 1.5 m. This value improves to less than 0.5 m if more corals (approximately 20) are sampled, especially if these have narrow living depth ranges. These tests can guide future coral sampling at other outcrops. After inferring RSL from the real coral elevations, we correct it for long-term uplift, using the elevation of the adjacent MIS 5e sea level outcrop to calculate an uplift rate of 0.522 ± 0.036 m/kyr (1σ), and for glacial isostatic adjustment. We find that GMSL most likely peaked at −22.3 m relative to present GMSL (−32.5 m to −10.7 m, 95% credible interval). This work provides a new estimate for MIS 5a GMSL that is lower than results from most previous studies, and confirms sequentially decreasing GMSL during the MIS 5e, 5c, and 5a precessional insolation peaks, indicating increased ice sheet growth and cooling into the ice age following the peak interglacial MIS 5e.

1. Introduction

Over past glacial-interglacial cycles, the sizes of ice sheets have fluctuated in response to climate forcing. Global mean sea level (GMSL) covaries with global ice volume, and GMSL reconstructions have therefore been powerful tools to investigate the sensitivity of ice sheets to past warming. Marine Isotope Stage 5 (MIS 5) spanned 130 to 71 ka, and benthic and planktonic oxygen isotope records indicate that this stage included three precession-paced warm periods (Lisiecki and Raymo, 2005; Shakun et al., 2015). MIS 5e (~130 to 115 ka) occurred first, and estimates of peak GMSL range from less than 5.3 m (Dyer et al., 2021) up to 9.4 m (Kopp et al., 2009) relative to the present day. Subsequently, MIS 5c occurred around 96 ka with a GMSL estimate of −9.4 ± 5.3 m (1σ, Creveling et al., 2017).

* Corresponding author. School of Earth and Ocean Sciences, University of Victoria, Victoria, British Columbia, V8P 5C2, Canada.
E-mail address: tawilmorsink@uvic.ca (K. Tawil-Morsink).

https://doi.org/10.1016/j.quascirev.2022.107783
0277-3791/

MIS 5a marks the last intermittent warm period before the much colder MIS 4 and occurred around 82 ka. An analysis of sea level records along the US Atlantic coast and the Caribbean indicated that GMSL was approximately −28 m below present (Potter and Lambeck, 2004) and that small sea level oscillations may have occurred during this interstadial (Potter et al., 2004). This estimate is in line with a global analysis by Lambeck and Chappell (2001). A slightly higher estimate of −23.5 m (or an alternative but less preferred estimate of −6.5 m if a different mantle viscosity is used) has been put forth by Muhs et al. (2012) based on a record from San Nicolas Island, California. Simms et al. (2016, 2020) find that a GMSL of −15.2 m or higher would be consistent with their data from the same region. The most recent study by Creveling et al. (2017) included global observations and inferred that GMSL was -10.5 ± 5.5 m (1σ, only considering data with robust age constraints). Lastly, Dorale et al. (2010) report a relatively high estimate of MIS 5a GMSL, which they argue was approximately 1 m above present-day sea level.

These studies demonstrate the large range of GMSL (and hence ice volume) estimates during MIS 5a, which represents an important gap in our knowledge. High GMSL during MIS 5a would imply a period of rapid melting at the end of MIS 5b (and rapid ice regrowth after MIS 5a) and possibly refute the dominance of the 100-kyr ice age cycle (Dorale et al., 2010). Low GMSL during MIS 5a could in turn indicate more stable and persistent ice sheets during late MIS 5 and a smoother (but still slightly oscillating) saw-tooth-like transition into the last ice age. Better constraining the evolution of GMSL during MIS 5a is therefore crucial for our understanding of how ice sheets respond to orbital forcing.

One strategy for reconstructing past GMSL is to infer ice volume change from the oxygen isotopic composition of marine microfossils in layered deep-sea sediments. However, the isotopic signal is influenced by other factors such as temperature and local hydrologic properties (Skinner and Shackleton, 2006; Shakun et al., 2015; Raymo et al., 2018) and does not map uniquely to ice volume, making this approach more suited to examining temporal patterns than inferring accurate GMSL. Alternatively, one can reconstruct GMSL by interpreting geologic indicators of past sea level such as beach deposits, wave-cut notches, phreatic overgrowths on speleothems, and coral reefs (Rovere et al., 2016). This approach is taken in the MIS 5a studies detailed above. Geologic reconstructions conventionally report the past local elevation of the ocean surface relative to the present-day local sea level, called relative sea level (RSL) (Shennan et al., 2015). To infer GMSL, RSL must be corrected for any process that causes deformation, which leads to a deviation between RSL and the global mean. One such process is glacial isostatic adjustment (GIA), which includes the viscoelastic deformational, rotational, and gravitational effects of the solid Earth that are driven by changes in the ice and ocean load. (We determined the two MIS 5a GMSL estimates from Muhs et al. (2012) that we reported above by adding to their reported RSL two GIA corrections they had based on two solid Earth models, yielding two different MIS 5a GMSL results.) Additional processes that act on longer time scales include tectonics, sediment loading, and changes in dynamic topography. We will group deformation that arises from these processes under the term long-term deformation. GIA and long-term deformation can both introduce significant uncertainties in GMSL estimates and may provide an explanation for the large range of existing MIS 5a GMSL estimates.

Here we use a fossil coral reef on the island of Barbados to obtain a new estimate of MIS 5a GMSL. The reef is extensive and exquisitely well-preserved, and has not been studied to date. Barbados has been the site of many glacial-interglacial sea level studies due to its well-preserved fossil coral reefs and its fast uplift, which enables the preservation of reef terraces from multiple glacial and interglacial periods (e.g., Broecker et al., 1968; Gallup et al., 1994; Schellmann et al., 2004; Radtke and Schellmann, 2006; Thompson and Goldstein, 2005). Barbados is part of the accretionary prism located at the convergent boundary where the Atlantic Ocean crust subducts underneath the Caribbean plate, which leads to continuous uplift (Brown and Westbrook, 1987). There are currently 18 or more uplifted fossilized coral reefs on Barbados, including reefs dating to MIS 5a (e.g., Bender et al., 1979; Speed and Cheng, 2004; Schellmann et al., 2004; Radtke and Schellmann, 2006).

The site of our reconstruction is on the west coast of the island and the outcrop can be traced laterally to other outcrops that have been assigned an MIS 5a age via radiometric dating (e.g., Speed and Cheng, 2004). Here we present results from dating one of the corals of this outcrop using U−Th disequilibrium to confirm the MIS 5a age. We further estimate MIS 5a RSL at this reef through Bayesian inference using the elevations of 222 individual corals along with the depth distributions of their species in the modern ocean. We use our inference scheme on a synthetic dataset to quantify how many corals (and what kind of species) are needed for a precise and accurate estimate of RSL. This information will be useful for determining sampling strategies at other outcrops at which corals can be identified at the species level. We correct our inferred RSL for long-term uplift and GIA to infer GMSL during MIS 5a.

2. Methods

2.1. Study site and coral elevations

Our field site is on the west coast of Barbados (close to the Mount Hillaby-Clermont Nose anticline) near the Usain Bolt Sports Complex of the Cave Hill School of Business, University of the West Indies (Fig. 1B). A coral terrace that is higher in elevation contacts a lower terrace at 13.13750°N, 59.63484°W. We interpret the lower terrace outcrop to be of MIS 5a age because it can be traced laterally to other outcrops that have been identified as MIS 5a via radiometric dating (Fig. 1C; Speed and Cheng, 2004). Additionally, the fossilized reef outcrop contains a large specimen of the coral *Pocillopora palmata*, which went extinct after MIS 5a (Fig. 2C; Toth et al., 2015). This coral's presence indicates that the reef grew no later than MIS 5a.

The fossilized reef at Cave Hill consists of a shoreline-perpendicular cross-section of the reef, which has been exposed by a road cut. The outcrop is slimmer towards the east, starting at around 1 m height, which increases to around 3 m at its western edge (Fig. 2A). At the outcrop's maximum height, the foot and head of the section are 21.2 m and 23.7 m above modern mean sea level (MSL), respectively. The top of the outcrop is slightly dipping inland and its westernmost area contains many specimens of *Acropora palmata* (Fig. 2). The majority of coral elevation data were collected from this area of the outcrop.

The reef cross-section features multiple large branching corals in growth position, many of them lacking the abrasion and secondary growths commonly seen in coral debris. Where the bases of these corals were visible, we noted intact holdfasts, diagnostic of *in situ* corals even in rotary cores (Stathakopoulos et al., 2020). The space between the large branching corals in the reef is filled by calcium carbonate sediment, other corals (either whole or broken into pieces), and the tests of other marine organisms such as sea urchins and bivalves. Fragments of *Acropora cervicornis* are abundant in the reef, especially in the upper section. We conclude from these observations that the reef was buried mostly intact, that the corals within the reef formed at approximately the same time, and that the large corals in growth position are *in situ*.

To analyze the outcrop and determine the elevation of a series of corals we produced a virtual 3D model of this section using

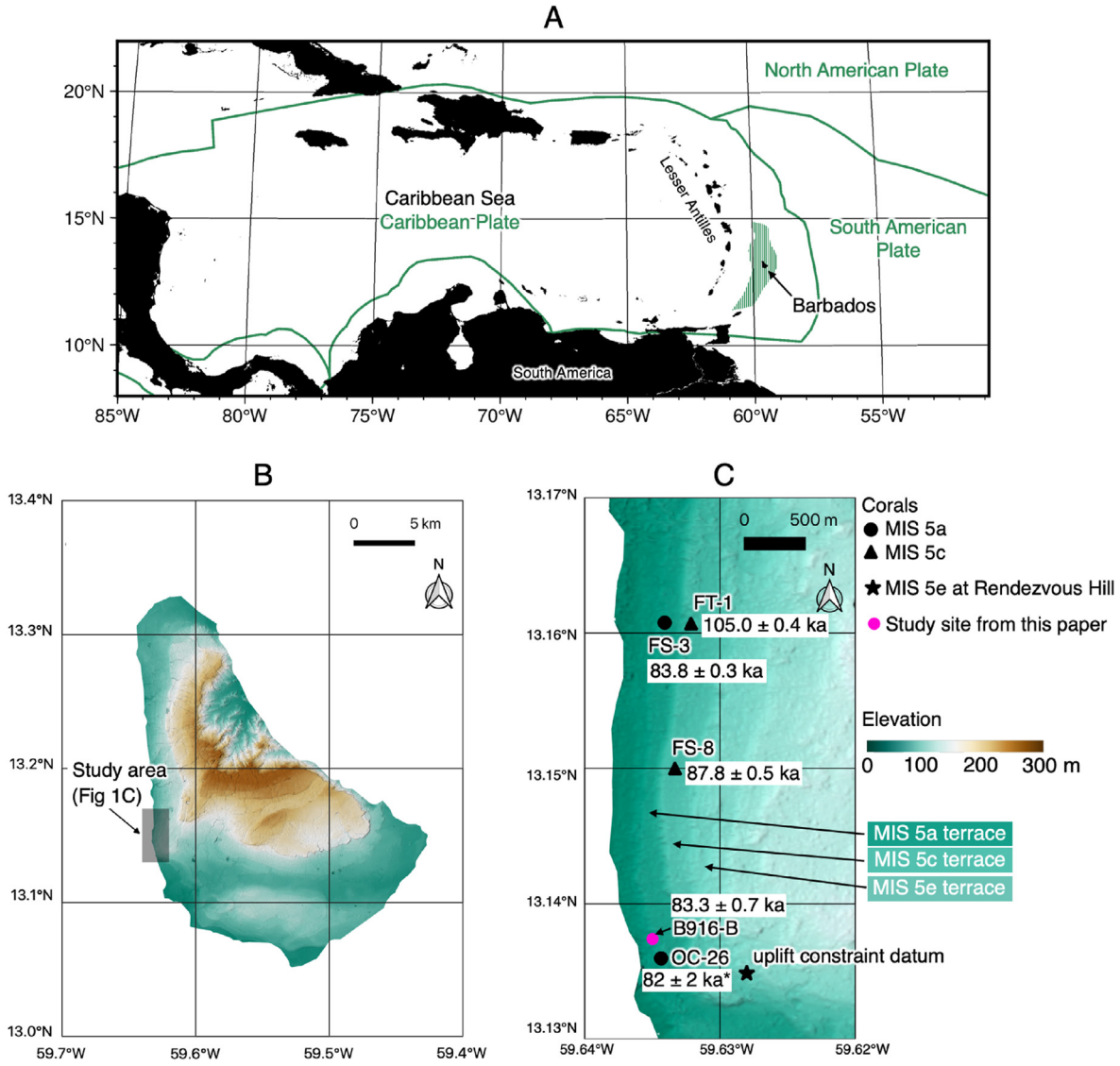

Fig. 1. (A) Regional map showing the location of the island of Barbados. Plate boundaries from Bird (2003) and plate names are shown in solid green. The uplift zone of the Barbados Ridge accretionary complex as mapped by Brown and Westbrook (1987) is hatched in green. (B) Topographic map of Barbados with the study area marked by grey rectangle (satellite-derived digital elevation data are from TanDEM-X, German Aerospace Center). (C) Topographic map of the study area highlighting the MIS 5a, 5c, and 5e terraces. Black circles mark the MIS 5a corals FS-3 and OC-26 and black triangles mark the MIS 5c corals FT-1 and FS-8 (Mesolella et al., 1969; Gallup et al., 1994). Hibbert et al. (2016) updated radiometric ages (with 2σ uncertainties), which are indicated for all these corals except OC-26, which appears only in Mesolella et al. (1969). This value has therefore been marked with an asterisk in panel C. Our study site is marked in pink and includes a newly dated *A. palmata* coral B916−B with open system age and 2σ uncertainty (Thompson et al., 2003). A black star marks the location of the uplift constraint datum used in this study, an MIS 5e shoreline angle at Rendezvous Hill (Speed and Cheng, 2004). (For interpretation of the references to color in this figure legend, the reader is referred to the Web version of this article.)

photogrammetry. We measured five high-resolution control points with differential GPS to georeference the 3D outcrop model. We then converted the vertical reference level from the WGS84 (World Geodetic System 84 also known as WGS, 1984; EPSG:4326) ellipsoid to a local estimate of elevation above MSL. We estimated local MSL on the WGS84 datum by measuring the middle of a modern tidal notch at Silver Sands Beach (-4.7 ± 0.5 m relative to WGS84, 1σ). We consider this offset between local MSL and WGS84 to be reasonable because in the nearby Bahamas MSLs are offset more than −30 m from WGS84 (Dyer et al., 2021). The uncertainty on our MSL estimate is intended to conservatively account for any possible discrepancy between the tidal notch midpoint and modern mean tide level, as well as the difference between mean tide level and mean sea level, which is estimated to be $\leq$ 1 cm on Barbados (Woodworth, 2017).

In the 3D model of the outcrop we determined the elevation of a series of corals that we considered to be *in situ* because they appeared to be well preserved and in growth position (Fig. 2). We picked 222 corals of three species (84 *A. palmata*, 124 *Siderastrea radians*, and 14 *Favia fragum*). We measured their elevations at the highest point that could be conservatively identified as part of the coral so that our RSL reconstruction would require that each entire coral grew underwater. Uncertainties in elevation relative to MSL were determined by taking the square root of the sum of the squared error on each elevation measurement ($1\sigma = 0.18$ m) and the uncertainty in our modern MSL ($1\sigma = 0.5$ m). The resulting combined uncertainty of $\pm$ 0.53 m (1σ) is mostly due to the uncertainty in the modern MSL estimate.

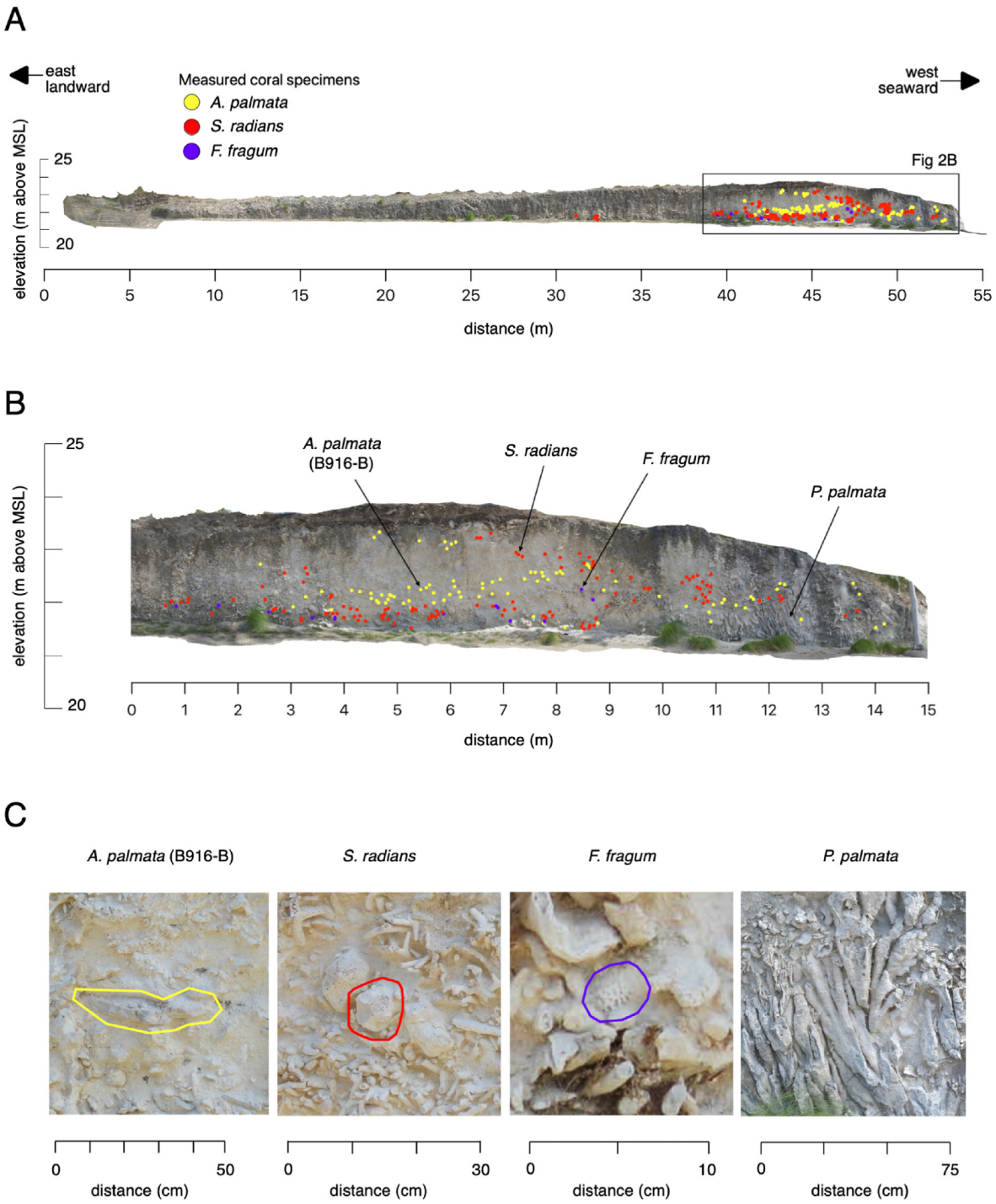

Fig. 2. (A) A two-dimensional orthorectified image of the lower terrace of the Usain Bolt Sports Complex road cut with identified specimens of *A. palmata*, *S. radians*, and *F. fragum* marked in yellow, red, and purple, respectively. (B) A two-dimensional orthorectified image of the part of the terrace where most coral specimens were measured (see panel A for location). (C) Insets showing fossilized specimens of *A. palmata*, *S. radians*, *F. fragum*, and *P. palmata*, whose locations are marked in (B). The *A. palmata* specimen shown is the specimen B916–B, which was used for radiometric dating. (For interpretation of the references to color in this figure legend, the reader is referred to the Web version of this article.)

2.2. U–Th methodology

We sampled a single *A. palmata* fossil coral towards the seaward side of the outcrop for U–Th disequilibrium analysis (Fig. 2B). We evaluated the degree of diagenesis of our sample based on its mineralogy, the ^{232}Th content, and $\delta^{234}U_i$. A detailed description of our screening protocol and preparation procedure is reported in Sandstrom (2021). After screening, we dissolved 200 mg of coral (99% aragonite) in HNO_3 and added a calibrated mixed ^{229}Th–^{233}U–^{236}U spike. U and Th were co-precipitated with iron and separated through standard ion exchange procedures using Bio-Rad AG 1 × 8200–400 mesh anion resin under ultra-clean conditions. Isotope ratios were determined using a multi-collector inductively coupled plasma mass spectrometer (ThermoScientific Neptune Plus) at Lamont-Doherty Earth Observatory, Columbia University. The age of our one *A. palmata* fossil coral was

calculated using a half-life of 75,584 yr for ^{230}Th and 245,620 yr for ^{234}U (Cheng et al., 2013).

2.3. Inferring RSL using Bayesian inference

RSL for each fossil coral in our outcrop is determined from the observed elevation of the coral above modern mean sea level, paired with the water depth distribution of the coral species in the present-day ocean based on Hibbert et al. (2016). Hibbert et al. (2016) used modern living depth data with vertical precision $\leq$ 0.25 m from the Ocean Biodiversity Information System (OBIS) database (OBIS, 2014) to define the depth distributions of 53 coral species, including *A. palmata*, *S. radians*, and *F. fragum*, the species for which we collected elevation data. The modern living depth data reported by Hibbert et al. (2016) are almost completely dominated by observations from the Caribbean and Gulf of Mexico: in the current version of the OBIS database, only 3 *S. radians* specimens are outside of this region (*Supplement*, Fig. S1; Table S1; OBIS, 2022). Although species-specific coral depth distributions do vary on sub-regional scales, the distribution of coral species across the Caribbean is less variable than in other parts of the world such as the Indo-Pacific (Hibbert et al., 2016; Veron et al., 2009). We assume that regional depth distributions of *A. palmata*, *S. radians*, and *F. fragum* are characteristic of those in Barbados. Also, multiple authors consider that the species makeup of Caribbean coral reefs has been generally constant over the last 1 million years (Hibbert et al., 2016; Budd et al., 1994; Mesolella, 1967; Jackson, 1992; Budd, 2000). This finding provides some support for our assumption that the *A. palmata*, *S. radians*, and *F. fragum* depth distributions were the same during MIS 5a as they are in the present.

In our model, we use modern living coral depth data to estimate the probability of finding a specific coral species at a given water depth. To characterize the depth distribution of each coral species, following Ashe et al. (2022), we create a nonparametric probability density function by applying a Gaussian kernel density estimation to the modern living depth data reported by Hibbert et al. (2016) (Fig. 3). In these data, there are many observations of *A. palmata* (n = 4760), so we expect that the *A. palmata* data are more complete than the data for *S. radians* (n = 275) and *F. fragum* (n = 230), which have wider depth ranges and fewer modern data points. We note that many environmental factors affect the zonation of coral species in reefs (Hibbert et al., 2016). The nonparametric fitting approach assumes the modern living depth data are complete enough to fully characterize the effects of these environmental factors. This approach yields a probability density distribution of water depth for each coral species based on modern observations. We cut off the distributions at 0 to enforce that corals do not grow above water. In our Bayesian inference, for each coral data point, the distribution corresponding to the species of that coral constitutes the prior for the distance between the coral and the sea surface. Assuming that all corals within the reef formed at the same time, all corals are responding to the same RSL, for which we assume a wide normally distributed prior (64 $\pm$ 36 m, 1σ). This RSL prior is centered on the elevation range between the highest measured coral elevation in the reef and 100 m above MSL, and conservatively covers a total range of possible RSL far beyond what is plausible.

In our model we calculate RSL by adding each coral's water depth to its measured elevation and enforcing that the RSL is common to all the corals. We determine the posterior common RSL using iterative sampling of priors and maximizing their likelihood (Hastings, 1970; Metropolis et al., 1953). Specifically, we sample priors using a Hamiltonian Monte Carlo method, the No U-Turn Sampler (NUTS) from the Bayesian statistical modeling package PyMC (Patil et al., 2010). In our sampling we ensure that every possible value that we generate for the posterior RSL is associated with its own set of possible posterior coral depths for the corals in the outcrop whose elevations we measured. To check for convergence, we informally inspect the sample traces to see that they are well-mixed, and we ensure they meet the criteria proposed by Geweke (1992) (within each chain of samples) and Gelman and Rubin (1992) (comparing chains of samples).

2.4. Tests with synthetic data to explore efficacy of different sampling strategies

We perform a series of tests using synthetic data to gain insight into the number and quality of sea level data needed to reliably infer RSL. We produce synthetic coral elevation data from 2 synthetic coral species, one of which has a narrow shallow depth distribution (0 to ~10 m, comparable to *A. palmata*), and the other of which has a wider, deeper distribution (~5 to ~35 m, Fig. 3). In addition to the water depth, we randomly pick a 'true' sea level to generate the synthetic coral elevations. After generating the synthetic data, we use them in our inference scheme as described above to produce an inferred sea level that we then compare to the true sea level. Ashe et al. (2022) used a similar approach to test their method of using nonparametric coral depth distributions to reconstruct rates of RSL change.

We performed 7070 inferences in which we vary the number of synthetic coral elevation data points used (from 1 to 70, increment of 1) and the proportion of elevation data points belonging to the shallow vs. deep coral species (from 0% to 100%, increment of 1%). We use our inference to reconstruct a posterior sea level for every combination of these two variables. We then evaluate the accuracy of the reconstruction as the offset between the true sea level used to generate the synthetic data and the most likely sea level yielded by the inference. We further evaluate the precision of the reconstruction as the width of the 68% credible interval of the posterior probability distribution for sea level.

2.5. Determination of MIS 5a GMSL

Once we have estimated RSL from our coral data, we can calculate GMSL by correcting for long-term uplift and deformation associated with GIA that have both occurred at the study site since the formation of the reef.

$$\text{GMSL} = \text{RSL} - (\text{uplift rate} \cdot \text{reef age}) - \text{GIA correction} \quad (1)$$

The uplift term that we calculate here is based on observations, which means it implicitly accounts for several geological processes. First, and most importantly, uplift of the island of Barbados over the last glacial-interglacial cycle is due to accretion of sediment at the convergent boundary between Atlantic Ocean crust and the Caribbean tectonic plate (Taylor and Mann, 1991; Torrini et al., 1985). Second, over the same time period, sediment loading has lessened the net uplift (Pico, 2020). Third, dynamic topography, i.e., differences in elevation on Earth's surface due to convection in the mantle, might have affected the elevation of Barbados since the last interglacial (Austermann et al., 2017).

Previous studies of Barbados' coral terraces have assumed that uplift has been constant through time at least since the last interglacial, or more specifically since the time of formation of Barbados' First High Cliff (Bender et al., 1979; Broecker et al., 1968; Cutler et al., 2003; Gallup et al., 1994, 2002; Matthews, 1973; Peltier and Fairbanks, 2006; Peltier et al., 2015; Radtke and Schellmann, 2006; Speed and Cheng, 2004). We make this same assumption and therefore calculate the uplift rate using an MIS 5e sea level observation on Barbados. Calculating the uplift rate requires the observed elevation and age of an MIS 5e sea level indicator paired

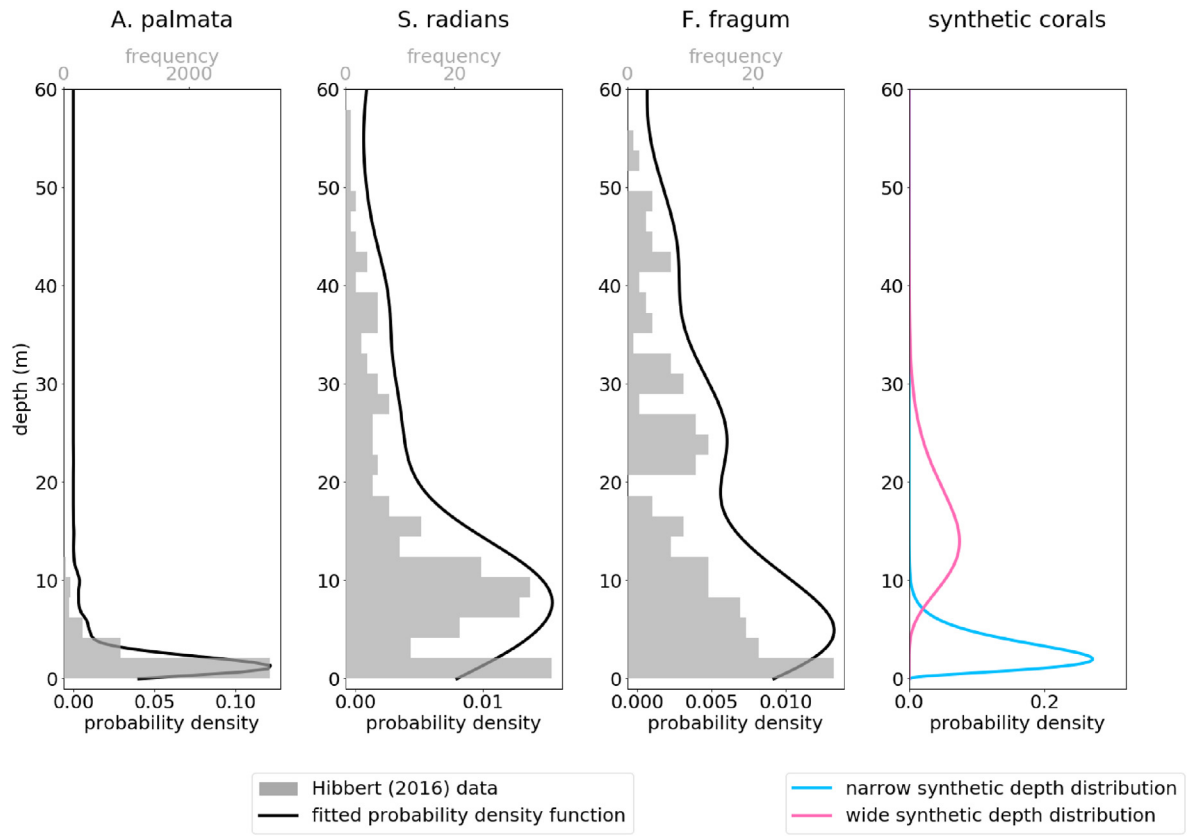

Fig. 3. Nonparametric probability density functions fitted to modern-day coral depth data from Hibbert et al. (2016). The number of modern coral observations in the compilation for *A. palmata*, *S. radians*, and *F. fragum* is 4760, 275, and 230, respectively. Depth distributions of synthetic coral species used in synthetic tests (one species with a narrow depth range, the other with a wide depth range) are shown on the right.

with the assumed RSL of that indicator during MIS 5e, i.e., its present-day location in the absence of uplift. (This assumed RSL is calculated based on a GMSL estimate and GIA prediction for MIS 5e.)

For our calculation of uplift rate in the Clermont Nose area, we use a shoreline angle documented by Speed and Cheng (2004) (about 800 m away from our study site) as an MIS 5e sea level indicator. This shoreline angle has an elevation of 70 ± 4 m (2σ, since the error is reported as ± 2 m unspecified) and an age of 120 ± 2 ka (2σ). Speed and Cheng (2004) argue that an estimate of a sustained MIS 5e highstand based on this shoreline angle would be more accurate than an estimate based on the highest dated coral, because coral reefs might grow during marine transgression, resulting in underestimation of the uplift rate when reef crest corals are used.

To determine MIS 5e RSL, we rely on results by Creveling et al. (2015), who used a GIA model to predict MIS 5e RSL in Barbados (without uplift) at the beginning and end of the last interglacial based on two different MIS 5e GMSL scenarios (6 m and 8 m GMSL). Estimates of last interglacial Barbados RSL were 4.96 m at the beginning and 7.63 m at the end in the first GMSL scenario, and 7.04 m at the beginning and 9.71 m at the end in the second GMSL scenario. The uplift rate since MIS 5e is then calculated as:

$$\text{uplift rate} = \frac{\text{MIS 5e indicator elevation} - \text{MIS 5e predicted RSL}}{\text{MIS 5e indicator age}} \quad (2)$$

We calculate a distribution of uplift rates by randomly sampling the indicator elevation and age based on their Gaussian distributions. For each sample we further use one of the 4 RSL predictions from Creveling et al. (2015). Note that when we randomly sample values this way, the age of the coral does not necessarily agree with the age at which the GIA correction was determined. However, the GIA correction is more uncertain than is explored here (e.g., due to uncertainties in the viscosity structure and past ice history; Dendy et al., 2017; Austermann et al., 2021) and therefore, considering the estimates by Creveling et al. (2015) as a spread for any given time is more conservative and appropriate.

Finally, we correct RSL for GIA. While sea level changes associated with GIA are largest in formerly glacial areas, GIA can still significantly alter RSL in tropical areas like Barbados (Austermann et al., 2013). GIA models require as input Earth's viscoelastic structure as well as the past ice history. Here we use results by Creveling et al. (2017), who found that for the U.S. East Coast and the Caribbean, existing sea level data from MIS 5a and 5c are fit best by an Earth structure with a lithospheric thickness of 95 km and an upper and lower mantle viscosity of 5×10^{20} Pa s and 4×10^{21} Pa s, respectively. They combine this Earth structure with 198 different ice histories, which differ in both the size and geometry of ice from 120 to 70 ka. This results in 198 GIA corrections, where the GIA correction is the deviation of RSL at our study site on Barbados relative to the global mean. We calculate the resulting MIS 5a GMSL for each correction, following equation (1). We next compare the inferred GMSL with the GMSL that is assumed in the ice history of the GIA correction. If the peak MIS 5a GMSL from the ice history falls within the 95% credible interval of the inferred GMSL, we consider the ice history to be consistent with our data. Note that this assumes that our coral reef grew during peak MIS 5a, which we

consider reasonable given the age, extent, and preservation of the outcrop. The distribution of GMSL estimates that are consistent with the GIA correction forms the result of our analysis.

3. Results

3.1. RSL reconstruction and synthetic tests

Based on the digitized outcrop, we identified and measured the elevations of 222 scleractinian corals. 84 corals are *A. palmata* and live at shallow water depth, while the remainder (124 *S. radians* and 14 *F. fragum*) have a slightly broader depth distribution and can live at deeper depths (Figs. 2 and 3). We note a close association of the upper limit of *A. palmata* in the outcrop with that of *in situ* colonies of the stony hydrocoral, *Millepora complanata*. This coral is a common indicator species of reef crest environments and can also serve as an excellent indicator of sea level, although we did not use it in our RSL reconstruction because the species is not documented in the Hibbert et al. (2016) compilation of modern coral depths. Using the elevation of the 222 corals combined with their water depths, we calculate a posterior MIS 5a RSL at the Cave Hill outcrop on Barbados. We find that RSL was most likely 23.7 m (22.7 − 24.8 m, 95% credible interval, Fig. 5A).

Our U–Th analysis of the *A. palmata* coral resulted in a $\delta^{234}U_i$ of 141 ± 1.4‰ (2σ), which is within the average range of modern corals/seawater (145 ± 5‰, 2σ) and is thus considered reliable (Chutcharavan et al., 2018). For this sample $^{234}U/^{238}U$ = 1.1133 ± 0.0011 and $^{230}Th/^{238}U$ = 0.5978 ± 0.0020, while ^{232}Th was negligible. These data yield a closed system age of the coral of 82.5 ± 0.4 ka and an open system age of 83.3 ± 0.7 ka (both uncertainties are 2σ), both of which indicate an MIS 5a origin of this outcrop (Thompson et al., 2003). Our age overlaps within uncertainty with MIS 5a coral FS-3 by Gallup et al. (1994), which has been reassessed by Hibbert et al. (2016) to give an age of 83.8 ± 0.3 ka (2σ), and coral OC-26 by Mesolella et al. (1969) (Fig. 1). (Mesolella et al. (1969) originally reported an age of 82.2 ± 2 ka for OC-26 and this age has not been reassessed.)

Our synthetic test results show how the accuracy and precision of the inferred sea level improves with an increasing number of corals and a greater proportion of corals with a narrow water depth distribution (Fig. 4). In reporting these results we refer to "narrow" corals from this narrow water depth distribution (coral living depth range 0 to ~10 m). The offset from true sea level (i.e., the accuracy) is relatively small (below 0.25 m) for most synthetic tests with a sample size of 30 or more corals and a "narrow" coral proportion of 35% or more (Fig. 4A). Note that we expect the real relationship between the number of corals sampled and accuracy to be smooth and change gradually, whereas the relationship shown in Fig. 4A is less smooth because it is limited by the number of trials and the chosen test-grid resolution. If there is a low proportion of "narrow" corals (less than 30%), the accuracy drops to less than 0.5 m, 0.75 m, or 1.5 m if 20–30, 5–20, or 0–5 corals are measured, respectively. If, however, "narrow" corals such as *A. palmata* are present and make up a significant proportion of the dataset (more than 50%), the accuracy is very good even if few (more than 5) corals are examined. This result is consistent with that of Ashe et al. (2022), who tested their method of using nonparametric coral depth distributions to reconstruct rates of RSL change and found that more synthetic *A. palmata* data produced more accurate results.

The precision, which we define here as the width of the 68% credible interval, is good (i.e., below 0.25 m) for most synthetic tests with a sample size of 30 or more corals and a "narrow" coral proportion larger than 45% (Fig. 4B). The trade-off between improving precision through increased number of samples or increased proportion of "narrow" corals is clearly visible. If only few or no "narrow" corals are available in an outcrop, the precision is below 0.75 m or 1.5 m if 10–40 or 0–10 corals are sampled, respectively. Analogously to the accuracy, if the proportion of "narrow" corals is high (more than 70%), a good precision of around 0.75 m or 0.5 m can be reached even if relatively few (5 or 10, respectively) corals are measured.

3.2. Global mean sea level during MIS 5a

Next we determine GMSL during MIS 5a by correcting RSL for long-term uplift and GIA. First, our uplift rates are close to normally distributed with a mean of 0.522 m/kyr and a standard deviation of 0.036 m/kyr (1σ). To calculate the amount of uplift, we multiply the rate by the age of the outcrop (see equation (1)), which we take as the open system age of the sampled *A. palmata* (83.3 ± 0.7 ka, 2σ). This results in a mean uplift of ~43.6 m since MIS 5a. Correcting RSL for this uplift and propagating uncertainties in the uplift rate and reef age leads to a most likely uplift-corrected RSL of −19.9 m (−25.7 to −13.8 m, 95% credible interval, Fig. 5A). Potter et al. (2004) estimated MIS 5a Barbados RSL as −19 ± 4 m for the highstand at ~84 ka, which is consistent with our uplift-corrected RSL estimate.

In our second step, we correct our sea level estimate for GIA. The GIA correction ranges from −10 m to +13 m with the most likely estimate around 4 m (Fig. 6). We found that 84 out of the 198 ice histories produced consistent GMSL results, i.e., an inferred GMSL that is consistent with the GMSL assumed in the GIA model. The consistent GIA corrections have a similar range and distribution to all GIA corrections (compare the dark to light green in Fig. 6). Correcting the uplift-corrected RSL for GIA yields a GMSL estimate of −22.5 m (−32.1 to −10.5 m, 95% credible interval) if all GIA corrections are considered and a similar value of −22.3 m (−32.5 to −10.7 m, 95% credible interval) if only the 84 consistent GIA corrections are used (Fig. 5B).

4. Discussion

Several estimates of MIS 5a GMSL that include both considerations of long-term deformation and GIA have been proposed, but vary significantly. Our best estimate of −22.3 m (−32.5 to −10.7 m, 95% credible interval, −27.9 to −16.4 m, 68% credible interval) agrees closely with the estimate of −23.5 m by Muhs et al. (2012), which they obtained by correcting RSL on San Nicolas Island, California, for long-term uplift and GIA using their preferred viscosity structure of upper and lower mantle viscosity of 5 × 10^{21} Pa s and 8 × 10^{21} Pa s, respectively. Our estimate is higher than that of ~ −28 m by Potter and Lambeck (2004), but their estimate overlaps with our 68% credible interval. In contrast, our estimates are significantly lower than the estimate of −10.5 ± 5.5 m (1σ, only using data with robust age control) by Creveling et al. (2017) (the 95% credible intervals of our estimates do not overlap). We note that sea level estimates from the Cave Hill region (however not our outcrop) were included in both the study by Potter and Lambeck (2004) and Creveling et al. (2017).

One possibility to reconcile our estimate with a higher MIS 5a GMSL sea level is that our outcrop is not recording peak sea level during MIS 5a. Suborbital variability within the highstand has been proposed including highstands at varying elevations (Potter and Lambeck, 2004; Potter et al., 2004). However, our open system coral age of 83.3 ± 0.7 ka (2σ) does coincide very well with the 65° insolation maximum at ~83.5 ka (Berger and Loutre, 1991). Additionally, the large extent of the reef, the size and density of *A. palmata*, and the gently sloping back reef flat inland of our outcrop support its formation at a highstand rather than during the transgression or regression. Another possibility to reconcile our

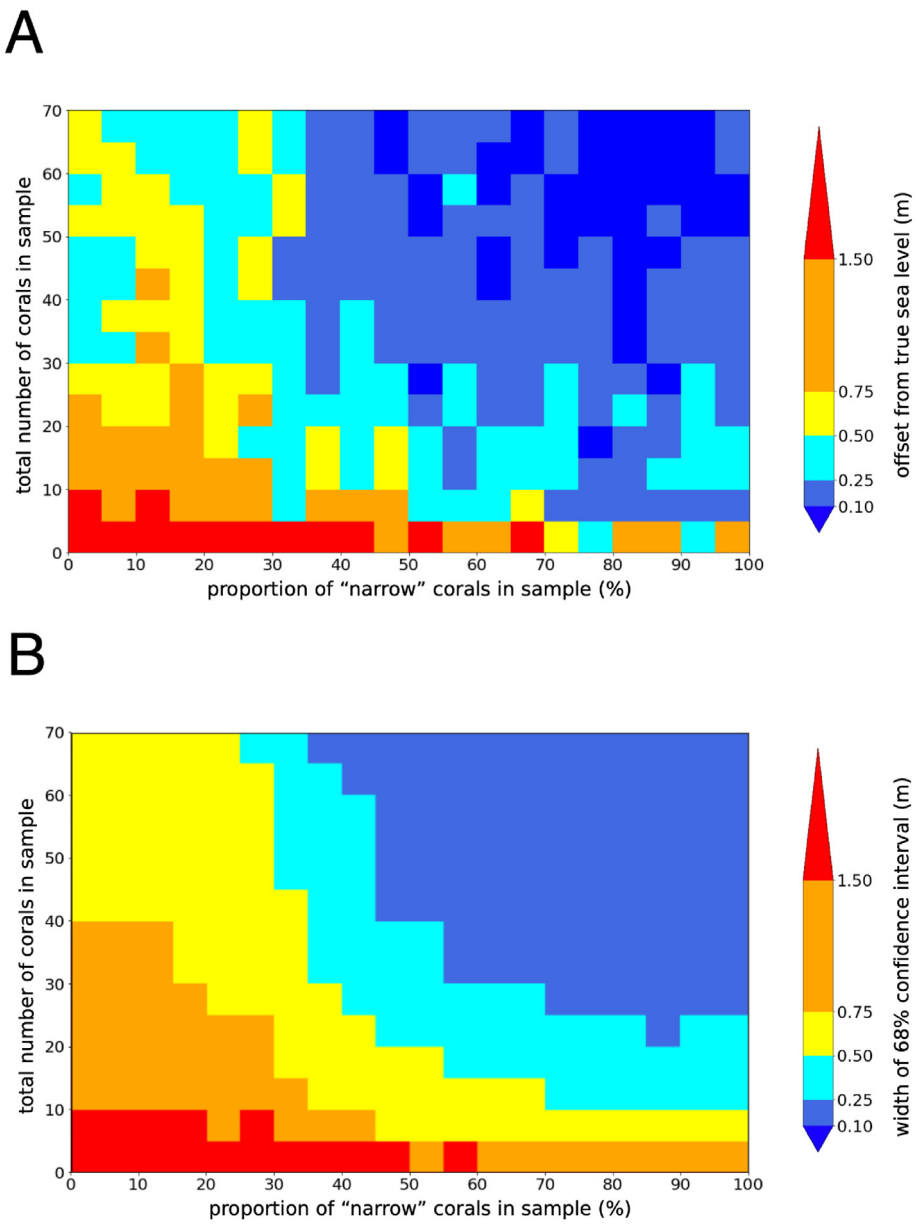

Fig. 4. (A) The offset between the sea level used to generate the synthetic data and the most likely sea level yielded by the inference - a measure of the method's accuracy - for different synthetic sample sizes ('total number of corals in the sample') and different proportions of elevation data points in the sample belonging to each species of coral ('proportion of "narrow" corals in the sample', where "narrow" corals have living depth range between 0 and ~10 m). (B) Same as (A), except that it shows the width of the 68% credible interval of the posterior probability distribution for sea level - a measure of the method's precision. In both graphs, the total number of corals in a sample is divided into increments of 5, the proportion of corals in a sample is divided into 5% increments, and the results in each group are averaged.

estimates with a higher GMSL is an overestimation of the uplift rate. Our uplift rate estimate is similar to the one obtained by Speed and Cheng (2004) (0.53 ± 0.02 m/kyr) but somewhat higher than others that have been calculated for the Clermont Nose area based on the highest dated *A. palmata* coral at Rendezvous Hill (~0.44 m/kyr; Matthews, 1973; Bender et al., 1979; Cutler et al., 2003). If we assume a lower uplift rate of approximately 0.44 m/kyr for the Clermont Nose area (rather than our estimate of 0.522 m/kyr), as determined using highest dated coral and terrace elevations by other authors (Matthews, 1973; Bender et al., 1979; Cutler et al., 2003; Peltier et al., 2015; Taylor and Mann, 1991), our GMSL estimate is increased by 6.8 m.

One general challenge with many MIS 5a studies, including ours, is that observations are focused around tectonically active margins, which requires a correction for tectonic offset (e.g. uplift). The common approach for studies in Barbados has been to infer uplift rates based on MIS 5e data. However, as detailed here, this approach introduces significant uncertainties, especially as GIA and GMSL during MIS 5e continue to be debated (Dyer et al., 2021; Austermann et al., 2021). Additionally, it requires the assumption that uplift has been constant in time, which might not hold (Radtke and Schellmann, 2006). A new global database of MIS 5a and MIS 5c sea level indicators has recently been published (Thompson and Creveling, 2021), and might allow investigating this assumption by testing inferences of GMSL using a variety of data subgroups to establish which observations (and hence which uplift corrections) might not be appropriate.

Deep sea oxygen isotope records provide complementary

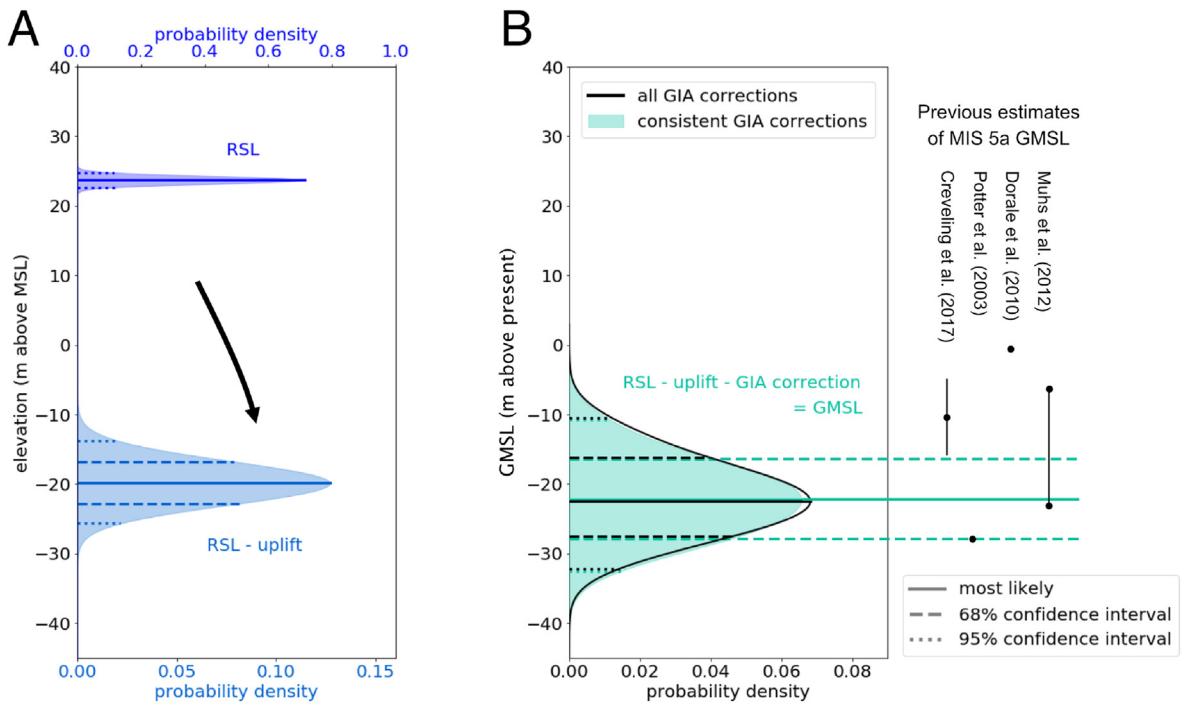

Fig. 5. (A) Probability density function of RSL as reconstructed from the Cave Hill coral reef (dark blue) and RSL after a correction for long-term uplift has been applied (light blue). (B) Probability density function of GMSL when the ensemble of all tested GIA corrections is used (black) and when the subset of all consistent GIA corrections is used (green). In each probability density function, the most likely result is indicated by a solid line, the 68% credible interval is indicated by dashed lines, and the 95% credible interval is indicated by dotted lines. Previous estimates of MIS 5a GMSL are shown to the right of panel B. Uncertainties by Creveling et al. (2017) are 1σ; Potter and Lambeck (2004) and Dorale et al. (2010) do not provide uncertainty estimates; the range shown for Muhs et al. (2012) spans their two estimates that vary by the GIA correction that is chosen. (For interpretation of the references to color in this figure legend, the reader is referred to the Web version of this article.)

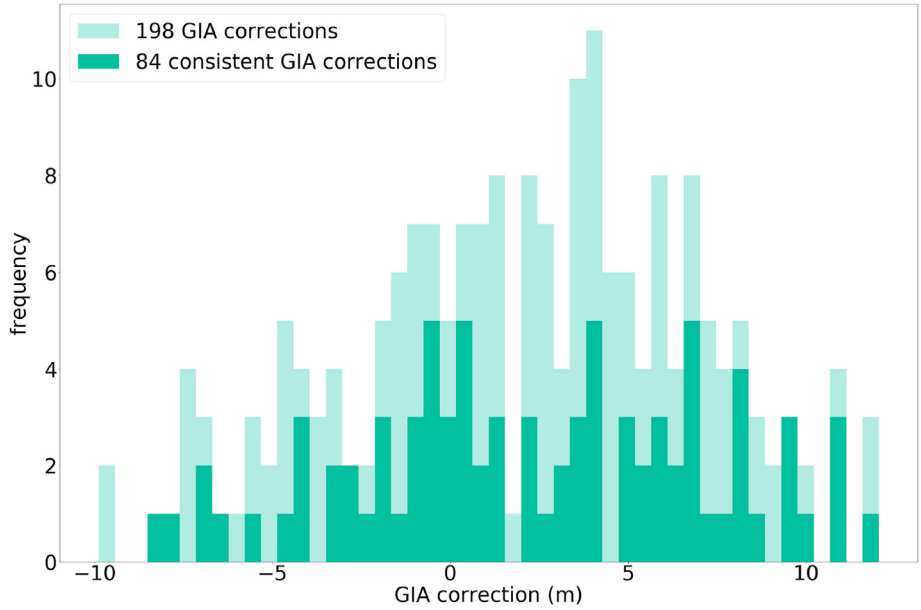

Fig. 6. Histogram of GIA corrections. Light green bars indicate all GIA corrections, while darker green bars are the subset of GIA corrections that produced a GMSL result consistent with the ice history that was modeled. In this study the GIA correction is the deviation of RSL at our study site on Barbados relative to the global mean. (For interpretation of the references to color in this figure legend, the reader is referred to the Web version of this article.)

estimates of past sea level variability (Lisiecki and Raymo, 2005). Waelbroeck et al. (2002) calibrated benthic foraminifera oxygen isotopic ratios from the North Atlantic and Equatorial Pacific Ocean with sea level records over the past glacial cycles and obtained an estimate of MIS 5a GMSL of around −30 m. An alternative approach is to use paired sea surface temperature-planktonic δ^{18}O records to correct for the contaminating effect of temperature on δ^{18}O. Using 49 such records, Shakun et al. (2015) have found that MIS 5a GMSL

was around −25 m. While inferring GMSL from oxygen isotopes is challenging (Raymo et al., 2018), it is interesting to note that these estimates agree well with our results.

5. Summary and conclusions

In this study we revisit the Cave Hill region of Barbados, which has been the focus of many studies that analyze sea level changes over past glacial cycles (e.g., Bender et al., 1979; Gallup et al., 1994, 2002; Thompson et al., 2003; Thompson and Goldstein, 2005; Schellmann et al., 2004; Speed and Cheng, 2004; Radtke and Schellmann, 2006). We describe and analyze a new outcrop of well-preserved fossilized coral reef of MIS 5a age. From this reef we sample and date one *A. palmata* coral, which returned an initial $\delta^{234}U_i$ of 141 ± 1.4‰ (2σ), a closed system age of 82.5 ± 0.4 ka (2σ) and an open system age of 83.3 ± 0.7 ka (2σ), i.e., a clear MIS 5a age (Thompson et al., 2003). Photogrammetry was used to produce a georeferenced 3D model of the outcrop, allowing us to pick 222 fossil coral elevations. We use these elevations to infer RSL using a Bayesian framework and find that it was 23.7 m (22.7 − 24.8 m, 95% credible interval).

We produce synthetic coral data to test our Bayesian inference scheme as well as explore how the number and type of corals in the dataset affect the accuracy and precision of the inferred sea level. This work showed that if possible, sampling the elevation of 5 corals, approximately half of which have a shallow living depth range, allows determining RSL with a precision and accuracy of around 1.5 m. Improvements can be made if more corals or a higher proportion of corals with a narrow living depth range (0 − ~10 m) are collected, and this paper quantifies the trade-offs in these parameters.

We correct the RSL estimate for long-term uplift and GIA to infer GMSL during MIS 5a and find that GMSL was −22.3 m (−32.5 to −10.7 m, 95% credible interval). This result is in line with some past estimates (Muhs et al., 2012; Shakun et al., 2015), but also higher (Lambeck and Chappell, 2001; Potter and Lambeck, 2004; Waelbroeck et al., 2002) and lower (Creveling et al., 2017) than others. Notably, Creveling et al. (2017) found that GMSL was similar during MIS 5c (−9.4 ± 5.3 m, 1σ) and MIS 5a (−8.5 ± 4.6 m, 1σ), and Dorale et al. (2010) have used speleothem encrustations from coastal caves on the island of Mallorca to argue that MIS 5a GMSL was around present-day values. Their findings have challenged the ice age sawtooth paradigm of a slow deglaciation from 115 ka to the last glacial maximum followed by a fast deglaciation. By contrast, our findings fit into this sawtooth paradigm. Our GMSL result is consistent with sequentially decreasing GMSL during the MIS 5e, 5c, and 5a precessional insolation peaks. It indicates that sea level during MIS 5a was significantly lower than present-day sea level and that ice volumes had already regrown by about 17% of their eventual last glacial maximum extent even at this intermittent warm period.

Author contributions

MER, SLG, BD, MC, and JA performed the fieldwork. MER initiated the project. SLG led the field trip by the group to Barbados. BD led the photogrammetry and rendered the outcrop. KTM led and performed the majority of the work including identifying the corals (with input from WFP), conceiving and performing the statistical analysis (with input from BD), and performing the GIA and sea level analysis (with input from JA). An early version of this work appeared as KTM's undergraduate thesis project at Columbia University. MC and OAD dated the coral with guidance from SLG. KTM wrote the majority of the manuscript with help from JA and BD and input from all co-authors.

Declaration of competing interest

The authors declare that they have no known competing financial interests or personal relationships that could have appeared to influence the work reported in this paper.

Acknowledgements

We thank J. Creveling and J.X. Mitrovica for providing their GIA results from Creveling et al. (2017). Alex Simms and one anonymous reviewer are thanked for their comments that improved the manuscript. J.A. acknowledges support from the Vetlesen Foundation. TanDEM-X digital elevation data used in Fig. 1 are under copyright by the German Aerospace Center. All rights reserved; used with permission within Project DEM GEOL1210 (Alessio Rovere and Maureen E. Raymo).

Appendix A. Supplementary data

Supplementary data to this article can be found online at https://doi.org/10.1016/j.quascirev.2022.107783.

References

Ashe, E.L., Khan, N.S., Toth, L.T., Dutton, A., Kopp, R.E., 2022. A statistical framework for integrating nonparametric proxy distributions into geological reconstructions of relative sea level. Adv. Stat. Climatol. Meteorol. Oceanogr. 8 (1), 1–29.

Austermann, J., Mitrovica, J.X., Latychev, K., Milne, G.A., 2013. Barbados-based estimate of ice volume at Last Glacial Maximum affected by subducted plate. Nat. Geosci. 6 (7), 553–557.

Austermann, J., Mitrovica, J.X., Huybers, P., Rovere, A., 2017. Detection of a dynamic topography signal in last interglacial sea-level records. Sci. Adv. 3 (7), e1700457.

Austermann, J., Hoggard, M.J., Latychev, K., Richards, F.D., Mitrovica, J.X., 2021. The effect of lateral variations in Earth structure on Last Interglacial sea level. Geophys. J. Int. 227 (3), 1938–1960.

Bender, M.L., Fairbanks, R.G., Taylor, F.W., Matthews, R.K., Goddard, J.G., Broecker, W.S., 1979. Uranium-series dating of the pleistocene reef tracts of Barbados, West Indies. Bull. Geol. Soc. Am. 90 (6), 577–594.

Berger, A., Loutre, M., 1991. Insolation values for the climate of the last 10 million years. Quat. Sci. Rev. 10 (4), 297–317.

Bird, P., 2003. An updated digital model of plate boundaries. G-cubed 4.

Broecker, W.S., Thurber, D.L., Goddard, J., Ku, T.L., Matthews, R.K., Mesolella, K.J., 1968. Milankovitch hypothesis supported by precise dating of coral reefs and deepsea sediments. Science 159 (3812), 297–300.

Brown, K.M., Westbrook, G.K., 1987. The tectonic fabric of the Barbados Ridge accretionary complex. Mar. Petrol. Geol. 4 (1), 71–81.

Budd, A.F., 2000. Diversity and extinction in the Cenozoic history of Caribbean reefs. Coral Reefs 19 (1), 25–35.

Budd, A.F., Stemann, T.A., Johnson, K.G., 1994. Stratigraphic distributions of genera and species of Neogene to Recent Caribbean reef corals. J. Paleontol. 68 (5), 951–977.

Cheng, H., Lawrence Edwards, R., Shen, C.C., Polyak, V.J., Asmerom, Y., Woodhead, J., Hellstrom, J., Wang, Y., Kong, X., Spötl, C., Wang, X., Calvin Alexander, E., 2013. Improvements in 230Th dating, 230Th and 234U half-life values, and U-Th isotopic measurements by multi-collector inductively coupled plasma mass spectrometry. Earth Planet Sci. Lett. 371–372, 82–91.

Chutcharavan, P.M., Dutton, A., Ellwood, M.J., 2018. Seawater 234U/238U recorded by modern and fossil corals. Geochem. Cosmochim. Acta 224, 1–17.

Creveling, J.R., Mitrovica, J.X., Hay, C.C., Austermann, J., Kopp, R.E., 2015. Revisiting tectonic corrections applied to Pleistocene sea-level highstands. Quat. Sci. Rev. 111, 72–80.

Creveling, J.R., Mitrovica, J.X., Clark, P.U., Waelbroeck, C., Pico, T., 2017. Predicted bounds on peak global mean sea level during marine isotope stages 5a and 5c. Quat. Sci. Rev. 163, 193–208.

Cutler, K.B., Edwards, R.L., Taylor, F.W., Cheng, H., Adkins, J., Gallup, C.D., Cutler, P.M., Burr, G.S., Bloom, A.L., 2003. Rapid sea-level fall and deep-ocean temperature change since the last interglacial period. Earth Planet Sci. Lett. 206 (3–4), 253–271.

Dendy, S., Austermann, J., Creveling, J., Mitrovica, J., 2017. Sensitivity of Last Interglacial sea-level high stands to ice sheet configuration during Marine Isotope Stage 6. Quat. Sci. Rev. 171, 234–244.

Dorale, J.A., Onac, B.P., Fornós, J.J., Ginés, J., Ginés, A., Tuccimei, P., Peate, D.W., 2010. Sea-level highstand 81,000 years ago in Mallorca. Science 327 (5967), 860–863.

Dyer, B., Austermann, J., D'Andrea, W.J., Creel, R.C., Sandstrom, M.R., Cashman, M., Rovere, A., Raymo, M.E., 2021. Sea-level trends across the Bahamas constrain peak last interglacial ice melt. Proc. Natl. Acad. Sci. USA 118 (33), e2026839118.

Gallup, C.D., Edwards, R.L., Johnson, R.G., 1994. The timing of high sea levels over the past 200,000 years. Science 263 (5148), 796–800.
Gallup, C.D., Cheng, H., Taylor, F.W., Edwards, R.L., 2002. Direct determination of the timing of sea level change during Termination II. Science 295 (5553), 310–313.
Gelman, A., Rubin, D., 1992. A Single Series from the Gibbs Sampler Provides a False Sense of Security. Oxford University Press, pp. 625–631.
Geweke, J., 1992. Evaluating the Accuracy of Sampling-Based Approaches to Calculating Posterior Moments. Oxford University Press, pp. 169–193.
Hastings, W.K., 1970. Monte Carlo sampling methods using Markov chains and their applications. Biometrika 57 (1), 97.
Hibbert, F.D., Rohling, E.J., Dutton, A., Williams, F.H., Chutcharavan, P.M., Zhao, C., Tamisiea, M.E., 2016. Coral indicators of past sea-level change: a global repository of U-series dated benchmarks. Quat. Sci. Rev. 145, 1–56.
Jackson, J.B., 1992. Pleistocene perspectives on coral reef community structure. Integr. Comp. Biol. 32 (6), 719–731.
Kopp, R.E., Simons, F.J., Mitrovica, J.X., Maloof, A.C., Oppenheimer, M., 2009. Probabilistic assessment of sea level during the last interglacial stage. Nature 462 (7275), 863–867.
Lambeck, K., Chappell, J., 2001. Sea Level Change through the Last Glacial Cycle.
Lisiecki, L.E., Raymo, M.E., 2005. A Pliocene-Pleistocene stack of 57 globally distributed benthic δ18O records. Paleoceanography 20 (1) (n/an/a).
Matthews, R.K., 1973. Relative elevation of late Pleistocene high sea level stands: Barbados uplift rates and their implications. Quat. Res. 3 (1), 147–153.
Mesolella, K.J., 1967. Zonation of uplifted pleistocene coral reefs on Barbados, West Indies. Science 156 (3775), 638–640.
Mesolella, K.J., Matthews, R.K., Broecker, W.S., Thurber, D.L., 1969. The astronomical theory of climatic change: Barbados data. J. Geol. 77 (3), 250–274.
Metropolis, N., Rosenbluth, A.W., Rosenbluth, M.N., Teller, A.H., Teller, E., 1953. Equation of state calculations by fast computing machines. J. Chem. Phys. 21 (6), 1087–1092.
Muhs, D.R., Simmons, K.R., Schumann, R.R., Groves, L.T., Mitrovica, J.X., Laurel, D.A., 2012. Sea-level history during the Last Interglacial complex on San Nicolas Island, California: implications for glacial isostatic adjustment processes, paleozoogeography and tectonics. Quat. Sci. Rev. 37, 1–25.
OBIS, 2014. Data from the Ocean Biogeographic Information System. Intergovernmental Oceanographic Commission of UNESCO. www.obis.org.
OBIS, 2022. Data from the Ocean Biogeographic Information System. Intergovernmental Oceanographic Commission of UNESCO. www.obis.org.
Patil, A., Huard, D., Fonnesbeck, C.J., 2010. PyMC: Bayesian stochastic modelling in Python. J. Stat. Software 35 (4), 1–81.
Peltier, W.R., Fairbanks, R.G., 2006. Global glacial ice volume and Last Glacial Maximum duration from an extended Barbados sea level record. Quat. Sci. Rev. 25 (2324), 3322–3337.
Peltier, W.R., Argus, D.F., Drummond, R., 2015. Space geodesy constrains ice age terminal deglaciation: the global ICE-6G_C (VM5a) model. J. Geophys. Res. Solid Earth 120, 450–487.
Pico, T., 2020. Towards assessing the influence of sediment loading on Last Interglacial sea level. Geophys. J. Int. 220 (1), 384–392.
Potter, E.-K., Lambeck, K., 2004. Reconciliation of sea-level observations in the Western North Atlantic during the last glacial cycle. Earth Planet Sci. Lett. 217 (1–2), 171–181.
Potter, E.-K., Esat, T.M., Schellmann, G., Radtke, U., Lambeck, K., McCulloch, M.T., 2004. Suborbital-period sea-level oscillations during marine isotope substages 5a and 5c. Earth Planet Sci. Lett. 225 (1–2), 191–204.
Radtke, U., Schellmann, G., 2006. Uplift history along the Clermont Nose traverse on the west coast of Barbados during the last 500,000 Years - implications for paleo-sea level reconstructions. J. Coast Res. 22 (2), 350–356.
Raymo, M.E., Kozdon, R., Evans, D., Lisiecki, L., Ford, H.L., 2018. The accuracy of mid-Pliocene δ18O-based ice volume and sea level reconstructions. Earth Sci. Rev. 177, 291–302.
Rovere, A., Raymo, M.E., Vacchi, M., Lorscheid, T., Stocchi, P., Gómez-Pujol, L., Harris, D.L., Casella, E., O'Leary, M.J., Hearty, P.J., 2016. The analysis of Last Interglacial (MIS 5e) relative sea-level indicators: Reconstructing sea-level in a warmer world.
Sandstrom, R.M., 2021. Geochronology and reconstruction of Quaternary and Neogene sea-level highstands. Columbia University. https://doi.org/10.7916/d8-1xn4-vb62.
Schellmann, G., Radtke, U., Potter, E.-K., Esat, T., McCulloch, M., 2004. Comparison of ESR and TIMS U/Th dating of marine isotope stage (MIS) 5e, 5c, and 5a coral from Barbados—implications for palaeo sea-level changes in the Caribbean. Quat. Int. 120 (1), 41–50.
Shakun, J.D., Lea, D.W., Lisiecki, L.E., Raymo, M.E., 2015. An 800-kyr record of global surface ocean δ18O and implications for ice volume-temperature coupling. Earth Planet Sci. Lett. 426, 58–68.
Shennan, I., Long, A.J., Horton, B.P. (Eds.), 2015. Handbook of Sea-Level Research. John Wiley & Sons, Ltd.
Simms, A.R., Rouby, H., Lambeck, K., 2016. Marine terraces and rates of vertical tectonic motion: the importance of glacio-isostatic adjustment along the Pacific coast of central North America. Bull. Geol. Soc. Am. 128 (1–2), 81–93.
Simms, A.R., Rood, D.H., Rockwell, T.K., 2020. Correcting MIS5e and 5a sea-level estimates for tectonic uplift, an example from southern California. Quat. Sci. Rev. 248, 106571.
Skinner, L.C., Shackleton, N.J., 2006. Deconstructing Terminations I and II: revisiting the glacioeustatic paradigm based on deep-water temperature estimates. Quat. Sci. Rev. 25 (23–24), 3312–3321.
Speed, R.C., Cheng, H., 2004. Evolution of marine terraces and sea level in the last interglacial, Cave Hill, Barbados. Bull. Geol. Soc. Am. 116 (1–2), 219–232.
Stathakopoulos, A., Riegl, B.M., Toth, L.T., 2020. A revised Holocene coral sea-level database from the Florida reef tract, USA. PeerJ 2020 (1), e8350.
Taylor, F.W., Mann, P., 1991. Late Quaternary folding of coral reef terraces, Barbados. Geology 19 (2), 103–106.
Thompson, S.B., Creveling, J.R., 2021. A global database of marine isotope substage 5a and 5c marine terraces and paleoshoreline indicators. Earth Syst. Sci. Data 13 (7), 3467–3490.
Thompson, W.G., Goldstein, S.L., 2005. Open-system coral ages reveal persistent suborbital sea-level cycles. Science 308 (5720), 401–404.
Thompson, W.G., Spiegelman, M.W., Goldstein, S.L., Speed, R.C., 2003. An open-system model for U-series age determinations of fossil corals. Earth Planet Sci. Lett. 210 (1–2), 365–381.
Torrini, R., Speed, R.C., Mattioli, G.S., 1985. Tectonic relationships between forearcbasin strata and the accretionary complex at Bath, Barbados. GSA Bull. 96 (7), 861.
Toth, L.T., Kuffner, I.B., Cheng, H., Lawrence Edwards, R., 2015. A new record of the late Pleistocene coral Pocillopora palmata from the Dry Tortugas, Florida reef tract, USA. Palaios 30 (12), 827–835.
Veron, J., Devantier, L.M., Turak, E., Green, A.L., Kininmonth, S., Stafford-Smith, M., Peterson, N., 2009. Delineating the coral triangle. Galaxea, J. Coral Reef Stud. 11 (2), 91–100.
Waelbroeck, C., Labeyrie, L., Michel, E., Duplessy, J., McManus, J., Lambeck, K., Balbon, E., Labracherie, M., 2002. Sea-level and deep water temperature changes derived from benthic foraminifera isotopic records. Quat. Sci. Rev. 21 (1–3), 295–305.
Woodworth, P.L., 2017. Differences between mean tide level and mean sea level. J. Geodes. 91.